arXiv:cond-mat/0407371v1 [cond-mat.mtrl-sci] 14 Jul 2004

Ferromagnetic resonance study of free hole contribution to magnetization and magnetic anisotropy in modulation-doped $Ga_{1-x}Mn_xAs/Ga_{1-y}Al_yAs$:Be

X. Liu, W. L. Lim, M. Dobrowolska, and J. K. Furdyna
Department of Physics, University of Notre Dame, Notre Dame, IN 46556

T. Wojtowicz
Department of Physics, University of Notre Dame and Institute of Physics, PAS, Warsaw, Poland

(Dated: February 2, 2008)

Ferromagnetic resonance (FMR) is used to study magnetic anisotropy of GaMnAs in a series of $Ga_{1-x}Mn_xAs/Ga_{1-y}Al_yAs$ heterostructures modulation-doped by Be. The FMR experiments provide a direct measure of cubic and uniaxial magnetic anisotropy fields, and their dependence on the doping level. It is found that the increase in doping – in addition to rising the Curie temperature of the $Ga_{1-x}Mn_xAs$ layers – also leads to a very significant increase of their uniaxial anisotropy field. The FMR measurements further show that the effective g-factor of $Ga_{1-x}Mn_xAs$ is also strongly affected by the doping. This in turn provides a direct measure of the contribution from the free hole magnetization to the magnetization of $Ga_{1-x}Mn_xAs$ system as a whole.

PACS numbers: 75.50.Pp, 76.30.-v, 76.50.+g, 75.70.Cn
Keywords: magnetic semiconductors, ferromagnetic resonance, magnetic anisotropy, modulation doping

Magnetic anisotropy in ferromagnetic (FM) semiconductors such as $Ga_{1-x}Mn_xAs$[1,2,3] is expected to play a key role in future spin-based devices based on these materials. Although it is now well established that the magnetic anisotropy of $III_{1-x}Mn_xV$ alloys originates from the anisotropy of the valence band,[4,5,6] the correlation between the magnetic anisotropy and the hole concentration is not yet well established.

It has recently been found that doping the $Ga_{1-y}Al_yAs$ barriers of $Ga_{1-x}Mn_xAs/Ga_{1-y}Al_yAs$ heterostructures by Be acceptors leads to a significant increase of the Curie temperature T_C of the $Ga_{1-x}Mn_xAs$ layer.[7] It was also shown that ferromagnetic resonance (FMR) can be used for directly determining the magnetic anisotropy of thin FM films.[8,9] In this paper we use FMR to show that magnetic anisotropy in ultra-thin modulation-doped GaMnAs films changes rapidly with doping level; and that the effective g-factor of GaMnAs is also strongly affected by the doping. This last finding directly reflects the contribution of the free hole magnetization to FMR dynamics.

Ferromagnetic $Ga_{1-x}Mn_xAs/Ga_{1-y}Al_yAs$ heterostructures were grown on semi-insulating (001) GaAs substrates by molecular beam epitaxy (MBE), as described in detail in Ref. 7. Three heterostructures were used in the current study, all three consisting of a 5.6 nm $Ga_{1-x}Mn_xAs$ layer ($x = 0.062$) followed by a 13.5 nm $Ga_{0.76}Al_{0.24}As$ barrier doped with Be starting at the distance of 1 monolayer away from the $Ga_{1-x}Mn_xAs$ layer. The Be flux was kept constant during the growth, but the thickness of the doped region d_{Be} was varied: $d_{Be} = 0$ (undoped control Sample #1), 5.3 nm (Sample #2) and 13.2 nm (Sample #3). The FMR measurements were carried out at 9.38 GHz using a Bruker electron paramagnetic resonance (EPR) spectrometer. The experimental set-up and the polar coordinate system used in the subsequent discussion were described in detail in Ref. 9. Each heterostructure was cleaved into three 2mm×2mm square pieces with edges along the [110] and [1$\bar{1}$0] directions, and the square pieces were mounted in the EPR bridge with the [1$\bar{1}$0], [110], or [010] directions pointing vertically. With the dc magnetic field **H** in the horizontal plane, this allowed us to map out the FMR for **H** at any angle θ_H between **H**‖[001] (normal to the layer plane) and three in-plane orientations: **H**‖[110], [1$\bar{1}$0], and [100], following the same procedure as in Ref. 9.

Because the GaMnAs layers under consideration are extremely thin ($\sim$ 6 nm), magnetization measurements by SQUID were found to be inaccurate. Instead, we made use of the fact that the anomalous Hall effect (AHE) is dominated by the magnetization M, and can thus serve as a measurement of that parameter. To obtain the value of M, in our analysis we assumed that AHE is dominated by side-jump scattering – i.e., that $M \propto R_{Hall}/R^2_{sheet}$, where R_{Hall} is the Hall resistance and R_{sheet} is the sheet resistance when **H** is applied perpendicular to the layer.[10] Typical magneto-transport data R_{Hall}/R^2_{sheet} are shown in Fig. 1 for several temperatures. Note that at T = 4.22K the magnetization saturates at fields of about 5 kOe for undoped material (upper panel), and at higher fields (above 6.5 kOe) for modulation-doped samples (bottom panel), indicating that the anisotropy field has been modified by the doping.

The inset in Fig. 2 shows FMR spectra at 4.0K for a modulation-doped GaMnAs/GaAlAs:Be film (sample #3) in four basic configurations: **H**‖[001], **H**‖[110], **H**‖ [1$\bar{1}$0], and **H**‖[100]. Strikingly, sharp FMR peaks are observed in all configurations (and persist up to T_C), indicating strong long-range FM coherence of the Mn^{++} spins. We find this remarkable, since the 5.6nm-thick $Ga_{0.94}Mn_{0.06}As$ film is equivalent to only one monolayer of Mn ions randomly distributed over the specimen. As shown in Fig. 2, for intermediate orientations of **H** between **H**‖[100] and **H**‖[001] the FMR peak H_R shifts from 1 kOe to 10 kOe. Additionally, an EPR peak is observed around 3.3 kOe for all field orientations, originating from a small fraction of isolated paramagnetic Mn^{++} ions with $g = 2.00$. By their strong dependence on crystal geometry, the FMR spectra in Fig. 2 thus establish, that magnetic anisotropy plays a major role in determining the fields at which the resonances occur.[11]

The magnetic anisotropy parameters of a GaMnAs film can be obtained by analyzing the angular dependence of H_R using the following equations and the coordinate system defined in Ref. 9. For $\varphi_H = 45°$ [$\mathbf{H}$ and $\mathbf{M}$ in the $(1\overline{1}0)$ plane],

$$\begin{aligned}
&(\omega/\gamma)^2 = [H_R \cos(\theta_H - \theta) + (-4\pi M + H_{2\perp} + H_{4\perp}/2\\
&-H_{4\|}/4)\cos 2\theta + (H_{4\perp}/2 + H_{4\|}/4)\cos 4\theta]\\
&\times[H_R \cos(\theta_H - \theta) + (-4\pi M + H_{2\perp} + H_{4\|}/2)\cos^2\theta\\
&+(H_{4\perp} + H_{4\|}/2)\cos^4\theta - H_{4\|}]; \qquad (1a)
\end{aligned}$$

and for $\varphi_H = 0°$ [$\mathbf{H}$ and $\mathbf{M}$ in the plane (010)],

$$\begin{aligned}
&(\omega/\gamma)^2 = [H_R \cos(\theta_H - \theta) + (-4\pi M + H_{2\perp} + H_{4\perp}/2\\
&-H_{4\|}/2)\cos 2\theta + (H_{4\perp}/2 + H_{4\|}/2)\cos 4\theta]\\
&\times[H_R \cos(\theta_H - \theta) + (-4\pi M + H_{2\perp} - 2H_{4\|})\cos^2\theta\\
&+(H_{4\perp} + H_{4\|})\cos^4\theta + H_{4\|}]. \qquad (1b)
\end{aligned}$$

Here $H_{2\perp}$ and $H_{4\perp}$ represent, respectively, the uniaxial and the cubic anisotropy fields perpendicular to the film; the anisotropy in the film plane is given by the cubic field $H_{4\|}$; ω is the angular microwave frequency; and $\gamma = g\mu_B\hbar^{-1}$ is the gyromagnetic ratio, g being the spectroscopic splitting factor and $\hbar$ the Planck constant. To simplify the analysis, we have ignored the small in-plane uniaxial anisotropy field $H_{2\|}$ associated with the difference between the $[1\overline{1}0]$ and [110] axes.[12]

To determine the parameters appearing in Eq. (1), we first analyze the highly-precise values of FMR fields H_R for the three high-symmetry directions ($\mathbf{H}$ parallel to [100], [110], and [001]).[9] An independent determination of the g-factor and the three anisotropy fields $H_{2\perp}$, $H_{4\|}$ and $H_{4\perp}$ could not be accomplished from the analysis of the these values of H_R alone without additional constraints, i.e., it was possible to find nearly identical fits for several values of g and anisotropy fields within experimental error. To reduce the number of fitting parameters, we have first imposed the value of $g = 2.00$ that corresponds to individual Mn^{++} ions. With this constraint, the data for Sample #3 at 4 K yield unique solutions of $H_{2\perp}$ = -4319 Oe, $H_{4\|}$ = 739 Oe, and $H_{4\perp}$ = -1933 Oe. Using these values in Eq. (1), we then obtain the angular variation of H_R shown by the dashed line in Fig. 3. The dashed curves clearly depart from the data, indicating that the assumption of $g = 2.00$ was not valid.

On the other hand, we note that – due to the large compressive – the effect of the cubic $H_{4\perp}$ term is expected to be completely overshadowed by $H_{2\perp}$, and may be neglected. In our second approach we will therefore assume $H_{4\perp} = 0$, allowing g, $H_{4\|}$ and $H_{2\perp}$ as fitting parameters. With this approach, the data for Sample #3 yield $g = 1.80$, $H_{4\|}$ = 720 Oe and $H_{2\perp}$ = -5887 Oe. Using these values (and $H_{4\perp} = 0$) in from Eq. (1), an excellent fit to the angular variation of H_R is obtained, as shown by the solid curve in Fig. 3. We now use the above results as starting parameters to carry out a weighted nonlinear least squares fit to FMR positions for all values of θ_H, allowing all four parameters (g, $H_{4\|}$, $H_{2\perp}$, and $H_{4\perp}$) to vary. The results for Sample #3 are: $g = 1.80 \pm 0.02$, $H_{4\perp} = 8 \pm 110$ Oe, $H_{4\|} = 735.3 \pm 20$ Oe and $H_{2\perp} = -5764 \pm 90$ Oe. Not that the relation between the three anisotropy, $|H_{4\perp}| \ll |H_{4\|}| \ll |H_{2\perp}|$, confirms our assumption that $H_{4\perp}$ can be neglected as a first approximation. Comparing these rigorous results with the parameters obtained from H_R observed for the three high-symmetry orientations ($\mathbf{H}$ parallel to [100], [110], and [001]) under the assumption that $H_{4\perp} = 0$ shows that the two approaches lead to very similar values. In our analysis of the data observed as a function of temperature we will therefore use the simpler approach. Finally, we note that some anisotropy of the g-factor is expected in 2D quantum structures.[13,14] However, a fit obtained by replacing g with $g = (g_{\|}^2 \sin^2\theta + g_{\perp}^2 \cos^2\theta)^{1/2}$ cannot be distinguished from the fit with an isotropic g-factor. We have therefore accepted an isotropic g-factor as an adequate approximation.

Returning to Fig. 3, it is clear from the inset that this contribution of the holes to the g-factor is enhanced as hole concentration increases (i.e., the fits departs further from the $g = 2.00$ curves as the doping level increases). The fact that *all* our attempts to fit the data consistently lead to an effective g-factor smaller than 2.00 indicates a finite contribution of the orbital magnetic moment to the magnetization. This can be understood as follows. The total magnetization of GaMnAs has two components: a contribution from Mn^{++} ions, with their pure spin moment corresponding to $g = 2.00$; and the free hole contribution, which includes both spin and orbital parts. The magnetic moments of the hole spins are described by the Luttinger parameter κ. Since the *p*-*d* exchange integral $\beta N_0 > 0$ and $\kappa > 0$ are widely accepted for GaMnAs,[5] the moments of the holes align themselves in the same direction as the moments of the Mn^{++} ions. In contrast, the orbital part of the hole moment (determined by Landau diamagnetic currents) create, through the spin-orbit interaction, a magnetization opposite to that of Mn^{++} ions.[5] Thus the effective g-factor determining the precession of the total $\boldsymbol{M}$ is a weighted average of g-factors for the Mn-ion (g_{Mn}) and for the hole (g_h), described by the expression,[15]

$$g_{eff} = (M_{Mn} + M_h)/(M_{Mn}/g_{Mn} + M_h/g_h). \qquad (2)$$

Now in the modulation-doped heterostructures, we obtain a significant increase of the free hole concentration compared to “normal” GaMnAs, which automatically enhances their effect.[7] Owing to the antiferromagnetic *p*-*d* exchange in GaMnAs between Mn^{++} and the holes, the value of $g \approx 1.80$ can only be achieved by assuming that the magnetization of the free holes M_h is opposite to that of the Mn^{++} ions, and g_h is positive, as indeed predicted in Ref. 5. With this constraint, Eq. (2) gives $M_h \approx$ -$0.15 M_{Mn}$, $g_h \approx 5$, thus indicating that Landau currents make significant contributions to the magnetization of the free holes, and must therefore be taken into account in III-Mn-As materials.

The g-factors and related magnetic properties for T = 10K are listed in Table I for all three specimens under investigation. Although the sheet carrier densities p_s-Hall obtained from Hall measurements are not rigorously valid due to the AHE contribution, they nevertheless provide a useful indication of the *relative* level of the doping.[16] The values of the hole concentration obtained from T$_C$ using the mean field model,[7] p_v-MF, are also listed in Table I for comparison. One should note that the concentration of Mn (both substitutional and interstial) is the same in all samples, because deposition of the modulation-doped GaAlAs:Be layer *after* the GaMnAs layer does not affect the GaMnAs layer which was already in place.[7,10] The observed changes listed in Tabe I for all three samples – decrease of the g-factor with doping, enhancement of the uniaxial anisotropy field $H_{2\perp}$, and reduction of $H_{4\|}$ – can thus only be ascribed to changes in the hole concentration.

Measurements of FMR up to the Curie temperature T$_C$ enable us to determine temperature dependences of both the magnetic anisotropy fields and of the g-factor in the modulation doped samples. These quantities, obtained using the four basic FMR geometries shown in the inset in Fig. 2 and assuming $H_{4\perp} = 0$, are plotted in Fig. 4 for Samples #1 (undoped; open symbols) and #3 (modulation doped; solid symbols). As shown in Fig. 4(a), FMR occurs above the $g = 2.00$ resonance position (horizontal dash-dotted line) when **H** is perpendicular to the film, and below that position for in-plane **H** orientations. Shifts from the dash-dotted line gradually decrease – and eventually vanish – as one approaches T$_C$. But clearly the modulation-doped sample has a much stronger shift (the strongest shift observed in any GaMnAs samples studied by FMR) than the undoped sample when **H** is normal to the film, indicating a large increase of magnetic anisotropy due to the doping.

Figure 4(b) illustrates several basic features of magnetic anisotropy and its dependence on temperature and on the free hole concentration. First, we note that the cubic anisotropy fields decrease very rapidly with increasing T, while $H_{2\perp}$ drops off much more slowly. And second, modulation doping unambiguously increases the perpendicular uniaxial anisotropy field $H_{2\perp}$, while reducing the in-plane cubic field $H_{4\|}$. These observations are consistent with theoretical calculations predicting changes of magnetic anisotropy with hole concentration,[5] although at this point the agreement is only qualitative. Finally, changes of the g-factor seen in the inset – although not systematic generally – show a clear trend to decrease in doped samples below ∼60K. While these g-factor values are only approximate, the low-temperature decrease of the g-factor in the doped samples may reflect the fact that larger numbers of hole spins from the GaAlAs barrier will couple with Mn^{++} spins in GaMnAs as T decreases, thus increasing the effect of Landau diamagnetism on the overall magnetization.

In summary, the results reported in this paper clearly point to the crucial role which holes play in determining the magnetic anisotropy and the magnetization of Ga$_{1-x}$Mn$_x$As. It is especially important to note that magnetic anisotropy of III$_{1-x}$Mn$_x$V materials can be manipulated by controlling the hole concentration, thus providing a mechanism which may be employed in future device applications. Since the dependence of the magnetic anisotropy parameters on the free hole concentration is not yet well understood, further rigorous theoretical studies addressing this issue are clearly needed.

This work was supported by the DARPA SpinS Program, by the Director, Office of Science, Office of Basic Energy Sciences, and by NSF-NIRT Grant DMR02-10519.

---

[1] H. Ohno, Science **281**, 951 (1998).

[2] H. Ohno, J. Magn. Magn. Mater. **200**, 110 (1999) and reference therein.

[3] J. K. Furdyna, *et al.*, J. Korean Physical Society 42, S579 (2003).

[4] M. Abolfath, *et al.*, Phys. Rev. B **63**, 054418 (2001).

[5] T. Dietl, H. Ohno, and F. Matsukura, Phys. Rev. B **63**, 195205 (2001).

[6] M. Sawicki *et al.*, J. Superconductivity/Novel Magnetism **16**, 7 (2003); M. Sawicki, *et al.*, to be published in Phys. Rev. B.

[7] T. Wojtowicz, *et al.*, Appl. Phys. Lett. **83**, 4220 (2003).

[8] M. Farle, Rep. Prog. Phys. **61**, 755 (1998).

[9] X. Liu, Y. Sasaki, and J. K. Furdyna, Phys. Rev. B **67**, 205204 (2003).

[10] K. M. Yu, *et al.*, Appl. Phys. Lett. **84**, 4325 (2004).

[11] Y. Sasaki, *et al.*, J. Appl. Phys. **91**, 7484 (2002).

[12] U. Welp, *et al.*, Appl. Phys. Lett. (in press).

[13] P. Peyla, *et al.*, Phys. Rev. B **47**, 3783 (1993)

[14] R. Winkler, *et al.*, Phys. Rev. Lett. **85**, 4574 (2000).

[15] M. Rubinstein, *et al.*, J. Magnetism and Magnetic Materials **250,** 164 (2002).

[16] D. Ruzmetov, *et al.*, Phys. Rev. B **69**, 155207 (2004).

TABLE I: Key parameters for the $Ga_{1-x}Mn_xAs/Ga_{1-y}Al_yAs$ heterostructures modulation-doped by Be.

Sample #	1	2	3
Structure	GaMnAs/GaAlAs	GaMnAs/GaAlAs:Be	
d_{Be} (nm)	0	5.3	13.2
T_C (K)	72	85	95
p_v-MF (cm^{-3})	1.24×10^{20}	1.48×10^{20}	1.64×10^{20}
p_s-Hall (cm^{-2})	1.32×10^{14}	1.74×10^{14}	2.94×10^{14}
M^{10K} (emu/cm^3)	30.0	25.9	29.4
$H_{2\perp}^{10K}$ (Oe)	-3734	-5560	-5924
$H_{4\parallel}^{10K}$ (Oe)	827	471	557
g^{10K}	1.94	1.87	1.82

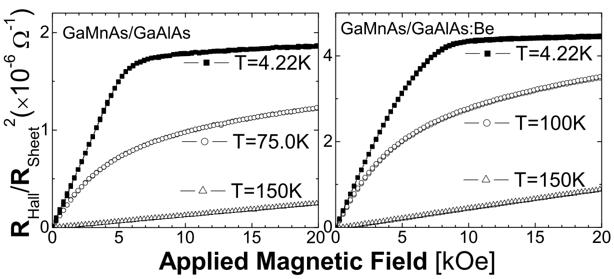

FIG. 1: Magnetization curves deduced from AHE at various temperatures for Samples #1 and #3. Magnetic field **H** is applied along the hard axis of magnetization, **H**||[001].

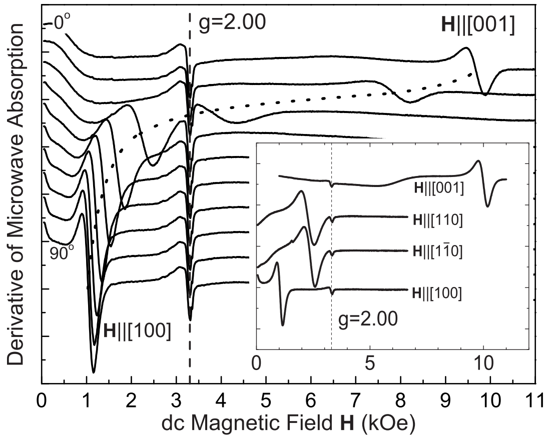

FIG. 2: FMR spectra (T = 4K) observed for Sample #3 at various orientations θ_H (from 0° to 90° in 10° increments) for **H** between [100] and [001] directions in the (010) plane. The dotted line is a guide for eyes, indicating the shifting FMR position. The insert shows FMR spectra for the perpendicular (**H**||[001]) and three parallel (**H**||[110], **H**||[$1\bar{1}0$], and **H**||[100]) configurations observed at 4.0 K. The weak peaks observed at the $g = 2.00$ resonance position (indicated by the vertical dashed line) are ascribed to EPR of isolated paramagnetic Mn^{++} ions.

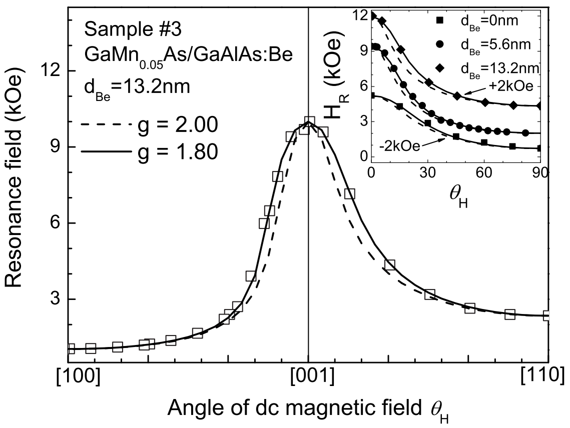

FIG. 3: Angular dependence of FMR positions for Sample #3 for **H** in the $(1\bar{1}0)$ plane (right-hand panel), and for **H** in the (010) plane (left-hand panel). Inset: Angular dependence of FMR positions at 4.0 K for **H** in the $(1\bar{1}0)$ plane for all three samples used in this study. Dashed curves show theoretical fits obtained for $g = 2.00$, $H_{4\perp} \neq 0$. The solid curves are fits obtained for $H_{4\perp} = 0$, $g = 1.80$ (main figure); and $H_{4\perp} = 0$, $g =$1.80, 1.87, and 1.92 (inset, top to bottom).

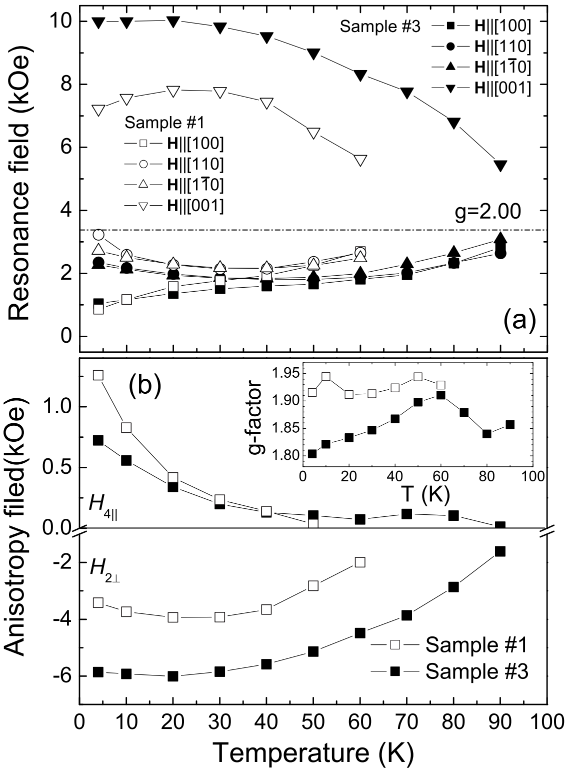

FIG. 4: Temperature dependence of the FMR results for undoped (Sample #1, open symbols) and modulation-doped (Sample #3, solid symbols) GaMnAs/GaAlAs heterostructures. Figure 4(a) shows FMR positions observed for the four basic orientations of **H** (same as in the inset in Fig.2). Figure 4(b) shows uniaxial anisotropy fields $H_{2\perp}$ for the two samples (bottom panel); cubic anisotropy fields $H_{4\parallel}$ (top panel); and the effective g-factors (inset).